

Highly Efficient Doping of Conjugated Polymers Using Multielectron Acceptor Salts

Gert Krauss, Adrian Hochgesang, John Mohanraj, and Mukundan Thelakkat*

Chemical doping is a vital tool for tuning electronic properties of conjugated polymers. Most single electron acceptors used for p-doping necessitate high dopant concentrations to achieve good electrical conductivity. However, high-molar doping ratios hamper doping efficiency. Here a new concept of using multielectron acceptor (MEA) salts as dopants for conjugated polymers is presented. Two novel MEA salts are synthesized and their doping efficiency towards two polymers differing in their dielectric properties are compared with two single electron acceptors such as NOPF₆ and magic blue. Cutting-edge methods such as ultraviolet photoelectron spectroscopy/X-ray photoelectron spectroscopy (XPS), impedance spectroscopy, and density of states analysis in addition to UV–vis–NIR absorption, spectroelectrochemistry, and Raman spectroscopy methods are used to characterize the doped systems. The tetracation salt improves the conductivity by two orders of magnitude and quadruples the charge carrier concentration compared to single electron acceptors for the same molar ratio. The differences in charge carrier density and activation energy on doping are delineated. Further, a strong dependency of the carrier release on the polymer polarity is observed. High carrier densities at reduced dopant loadings and improved doping efficacies using MEA dopants offer a highly efficient doping strategy for conjugated polymers.

example, in high-mobility OFETs,^[1–3] as novel thermoelectric materials^[4] or in organic photovoltaics.^[5,6] Inherently insulating conjugated polymers primarily require doping in order to achieve high electrical conductivity. During molecular doping, the conjugated polymer transfers electrons to the dopant (p-type doping leading to oxidized radical cation states) or back (n-type doping resulting in radical anion states). These redox processes introduce one preferred majority carrier type, e.g., holes in the case of p-doping and causes the shift of the Fermi level towards either valence band (p-doping) or conduction band (n-doping).^[7] Depending on the electronic structure and sterical demands of the host:dopant system, hybridization of the frontier orbitals with a concomitant formation of charge transfer complexes or redox reactions can be observed. The simplest doping mechanism is described by the integer charge transfer, where an integer number of electrons is transferred between the host and dopant. During p-type doping, the redox process occurs in which electrons are


transferred from highest occupied molecular orbital (HOMO) of the conjugated polymer to empty lowest unoccupied molecular orbital (LUMO) or partially filled singly occupied molecular orbital (SOMO) of the dopant.^[8] The most common p-type dopants are tetracyanoquinodimethane (F₄TCNQ)^[9–11] and its derivative, hexafluorotetracyanonaphthoquinodimethane (F₆TCNNQ).^[12] Other dopants are conventional oxidizing agents like iron(III)chloride (FeCl₃), nitrosonium tetrafluoroborate (NOBF₄) or nitrosonium hexafluorophosphate (NOPF₆),^[4,13,14] which are usually capable of accepting one electron per dopant molecule. This circumstance necessitates the employment of high dopant loadings in the range of 20 mol% or more in order to achieve appreciable electrical conductivities required for the intended application.^[11,15] By doping, the charge carrier concentration is increased and ideally the conductivity and charge carrier mobility are enhanced concurrently,^[16] predominantly in the low-doping regime (<1 mol%) due to filling of deep-lying trap states.^[17] On the other hand, it is accepted that excessive amounts of dopants have detrimental effects on the polymer microstructure and film morphology, leading to decreased charge transport properties.^[18–20] Lying dormant, the acceptor anions or the ionized dopant molecules act as Coulombic traps, i.e., charge carriers are temporarily bound by these trap

1. Introduction

In recent years, doped conjugated polymers have emerged into different areas of applications and the scientific interest in this field of research is unbroken. A variety of modern devices require doped conjugated polymers as their active materials, for

G. Krauss, A. Hochgesang, J. Mohanraj, M. Thelakkat
 Applied Functional Polymers, Macromolecular Chemistry I
 University of Bayreuth
 Bayreuth 95440, Germany
 E-mail: mukundan.thelakkat@uni-bayreuth.de

M. Thelakkat
 Bavarian Polymer Institute
 University of Bayreuth
 Bayreuth 95440, Germany

 The ORCID identification number(s) for the author(s) of this article can be found under <https://doi.org/10.1002/marc.202100443>

© 2021 The Authors. Macromolecular Rapid Communications published by Wiley-VCH GmbH. This is an open access article under the terms of the Creative Commons Attribution License, which permits use, distribution and reproduction in any medium, provided the original work is properly cited.

DOI: 10.1002/marc.202100443

states and contribute significantly less to the overall current.^[21] This problem is amplified by a rapidly decreasing doping efficiency with increasing doping ratio, meaning that less and less dopants participate in the desired redox reaction.^[8,22] As a consequence, the introduced molar dopant amounts need to be kept as low as possible to fully exploit the potential of both, high doping efficiency as well as good charge transport in the doped conjugated polymer. In this context, it is known that radical cation salts of hole transport materials (HTMs) such as spiro-MeOTAD²⁺(TFSI⁻)₂ or MeOTPD⁺(TFSI⁻) can be used as additives to the pristine spiro-MeOTAD (2,2',7,7'-Tetrakis[N,N-di(4-methoxyphenyl)amino]-9,9'-spirobifluorene) to redistribute the charges (comproportionation) and thus to improve the electrical conductivity of the latter.^[23–25] Inspired by this fact, we have earlier demonstrated the proof of principle of a highly thermally stable doping strategy for conjugated polymers where spiro-MeOTAD²⁺(TFSI⁻)₂ was employed for HOMO–HOMO electron transfer with a conjugated polymer.^[26] In a similar fashion, Hofmann et al. showed that a singly oxidized triarylammonium radical cation salt, tris(4-bromophenyl) ammonium hexachloroantimonate (Magic Blue), is capable of p-doping a variety of conjugated polymers.^[27] In most of these reported cases, only one electron is accepted by such a radical cation dopant molecule and therefore to achieve high conductivity high molar dopant ratio is required. Since spiro-MeOTAD can be theoretically oxidized to a tetracation salt and MeOTPD to its dication salt, here we ask a fundamental question on the efficacy of such multivalent radical cation salts as multielectron acceptors (MEAs). Our motivation is based on the idea that theoretically the tetracation salt of spiro-MeOTAD should exhibit the highest degree of doping for the same molar dopant ratio, if it can take up four electrons from the conjugated polymer. This can then fulfill the requirement of desired low doping levels, as explained earlier, if we can make use of multication salts. To study this, we chemically synthesized fully oxidized novel radical cation salts, spiro-MeOTAD⁴⁺(PF₆⁻)₄ and MeOTPD²⁺(PF₆⁻)₂ and addressed the feasibility and efficacy of using such multication salts (which are themselves HTMs) as MEA dopants for two different polydiketopyrrolopyrroles (PDPPs) differing in their polarity and dielectric constants. To quantify the results, we compare the properties of the doped systems with those doped with the well-known monoradical cation salts, magic blue as well as NOPF₆. We study in detail how the doping efficiency and the electronic properties of the doped polymers change. The three triphenylamine radical cation salts having oxidation states 1, 2, and 4 used here are: tris(4-bromophenyl)ammonium hexachloroantimonate (“Magic Blue”, D2), N,N,N',N'-tetrakis(4-methoxyphenyl)benzidine hexafluorophosphate (“MeOTPD²⁺(PF₆⁻)₂”, D3) and 2,2',7,7'-tetrakis[N-(4-methoxyphenyl)amino]-9,9'-spirobifluorene hexafluorophosphate (spiro-MeOTAD⁴⁺(PF₆⁻)₄ D4). Here the dication salt D3 and tetracation salt D4 are expected to have very similar electronic energies and absorption features, thus enabling a fair comparison of doping efficiency just based on their capacity to accept two or four electrons, respectively. Two DPP-based polymers with varying hydrophilicity, but similar electronic properties were selected as host materials to study the changes in electrical conductivity, charge carrier mobility and charge carrier density imparted by the different dopants in environments of different polarity. We address the following scientific questions in this work.

- 1) Can the tetracation dopant D4 (spiro-MeOTAD⁴⁺(PF₆⁻)₄) generate four times the charge carrier density compared to single electron acceptors, NOPF₆ or Magic Blue?
- 2) What are the consequences on electrical conductivity, charge carrier mobility and activation energy on using triphenylamine radical cation salts, which are themselves HTMs, as p-dopants compared with the conventional redox-dopant NOPF₆?
- 3) How does the polarity of the host polymer affect the doping process?

Here, the compatibility of dopant and host as a key requirement for efficient doping is studied using X-ray photoelectron spectroscopy (XPS) mapping. The electronic properties and energy levels of the dopants and polymers are assessed by ultraviolet photoelectron spectroscopy (UPS). The doping process is monitored using optical absorption spectroscopy as well as UPS. The electrical conductivity and thermal activation energy thereof are measured to study the impact of different dopants on macroscopic charge transport properties, depending on the polymer polarity and polarizability. To study the differences in charge carrier density in the doped polymers using mono-, di-, and tetracation salt dopants as compared to single electron oxidants and to determine the resulting doping efficiency, impedance spectroscopy experiments were performed. We also elucidated how HTM-dopants such as D3 and D4 differ on their influence on the charge carrier density, charge carrier mobility, activation energy for charge transport and density of states of doped polymers compared to a non-HTM dopant such as NOPF₆. Altogether, we present a comprehensive and comparative study of a series of triarylamine cation salt dopants with increasing oxidation state from 1 to 4 in two different DPP-polymers, thus highlighting the benefits and drawbacks, if any, of multiple oxidized triarylamine based HTM-dopants. Thereby, the electrical conductivity gained by doping with 5 mol% of a tetracation dopant spiro-MeOTAD⁴⁺(PF₆⁻)₄ is 255 times higher than that obtained with an equal molar amount of NOPF₆. Thus, we introduce an elegant concept for highly efficient doping of conjugated polymers using multielectron acceptors at unprecedented low dopant molar ratios, opening up innovative and novel p-doping strategies.

2. Results and Discussion

The chemical structures of all the dopants and conjugated polymers investigated in this work are displayed in **Figure 1a**. We studied two PDPPs with an identical backbone structure consisting of a thiophene-flanked DPP-core (DPP[T]₂) and 3-(2-(2-methoxyethoxy)ethoxy)thiophene (3-MEET) as comonomer. The presence of 3-MEET as comonomer helps to maintain a low ionization potential in the range of 4.6 eV.^[28] These are donor-acceptor polymers capable of undergoing p-doping.^[29,30] The DPP[T]₂ core is either equipped with hydrophilic triethylene glycol {TEG} substituents in the polymer PDPP[T]₂{TEG}₂-3-MEET denoted as P1, or hydrophobic 2-hexyldecyl {2-HD} chains in the polymer PDPP[T]₂{2-HD}₂-3-MEET, denoted as P2. Both polymers exhibit sufficient solubility in common organic solvents. Further, the replacement of the 2-HD substituents with TEG chains leads to an increase of the fraction of ethylene glycol from 13 to 52 wt%. Due to this, a difference

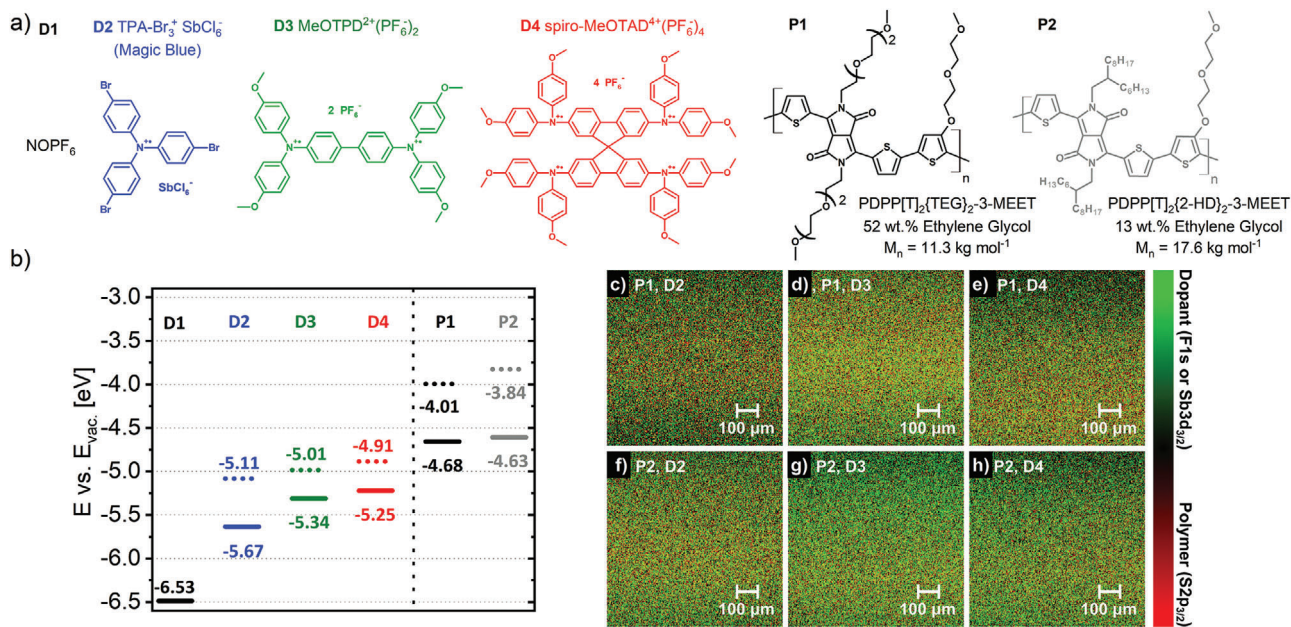


Figure 1. a) Structures of the studied dopants D1 (NOPF_6 , black), D2 (Magic Blue, blue), D3 ($\text{MeOTPD}^{2+}(\text{PF}_6)_2$, green), D4 ($\text{spiro-MeOTAD}^{4+}(\text{PF}_6)_4$, red) and the polymers P1 ($\text{PDPPP}[\text{T}_2\{\text{TEG}\}_2\text{-3-MEET}$, black) and P2 ($\text{PDPPP}[\text{T}_2\{2\text{-HD}\}_2\text{-3-MEET}$, gray). b) Ionization potentials (solid lines) and work function (dotted lines) of D2–D4, P1, and P2 w.r.t. vacuum level as obtained from UPS experiments. D1 value taken from ref. [35]. c)–h) XPS elemental maps of P1 and P2 doped with 5 mol% D2, D3, and D4 over an area of 750 by 750 μm featuring a lateral resolution of 10 μm . Colors represent the peak intensity of the mapped elements at a particular binding energy, which are exclusive to either polymer or dopant. P1 and P2 are attributed to their thiophene sulfur 2p $_{3/2}$ (165 eV, red) signal, D2 to the antimony 3d $_{3/2}$ (539 eV, green) signal, D3 and D4 to the fluorine 1s signal (688 eV, green).

in miscibility between the dopant salts and polymer can be expected and the dissociation of generated charge transfer state may be facilitated by the higher dielectric constant due to ethylene glycol groups. This may influence both charge carrier mobilities and electrical conductivities.^[11,31,32] The three HTM-dopants are based on the common basic structural motif triphenylamine and have different oxidation states. The singly oxidized Magic Blue (D2) carrying hexachloroantimonate as counter ion was purchased. The new dication salts, N,N,N',N' -tetrakis(4-methoxyphenyl)benzidine hexafluorophosphate (D3, $\text{MeOTPD}^{2+}(\text{PF}_6)_2$) and the tetracation salt, $2,2'',7,7''$ -tetrakis[N,N -di(4-methoxyphenyl)amino]-9,9'-spirobifluorene hexafluorophosphate (D4, $\text{spiro-MeOTAD}^{4+}(\text{PF}_6)_4$) were chemically synthesized by reacting the pristine molecules, MeOTPD and spiro-MeOTAD with carefully dried nitrosonium hexafluorophosphate in large molar excesses required for complete oxidation under extreme dry conditions under argon (see Supporting Information). UPS was conducted on thin film samples of P1, P2, and D2 to D4 on ITO to assess the HOMO energy levels and work functions (Figure S1, Supporting Information). From the energy diagram in Figure 1b it is apparent, that both polymers exhibit very similar ionization potentials of 4.6–4.7 eV, in accordance with the fact that the polymer backbones are identical, which dictate the HOMO energy levels. All three triarylamine dopants, D2 to D4 are thermodynamically capable of oxidizing the polymers, as their partially occupied HOMOs (5.7, 5.3, and 5.3 eV, respectively) lie well below those of the polymers. From the measured SOMO levels, the most exothermic electron transfer from polymer to dopant can be expected for D2, followed by D3 and D4. We postulate that the doping-mechanism

of the HTM-dopants occurs via integer charge transfer, as hybridization and the formation of charge-transfer complexes is unlikely in these sterically demanding dopants and nonplanar polymers.^[33,34] First we confirmed the uniform distribution of the dopants in our doped polymer thin films using an XPS mapping technique for 5 mol% D2, D3, and D4 (highest molar ratio) over an area of 0.56 mm 2 . By selecting binding energies which are exclusive to either the polymer (Thiophene sulfur 2p $_{3/2}$) or dopant (Antimony 3d $_{3/2}$ or Fluorine 1s), we could demonstrate a uniform distribution of D2 to D4 in both polymers with a lateral resolution of 10 μm (Figure 1d,e). High miscibility in both alkyl- and TEG side chain substituted polymers results in astonishing compatibility of our HTM dopants with semiconducting PDPP polymers. This also excludes inhomogeneities, which may otherwise will have to be considered in the electrical characterisations and interpretations of the resulting thin films.

2.1. Dopant Characterization

The triarylamine based cation salts D2–D4 were thoroughly characterized using additional spectroscopic methods such as UV/vis/NIR and Raman spectroscopy as given in Figures S2 and S3 of the Supporting Information, respectively. All the triarylamine dopants, D2–D4 feature an absorption at ≈ 700 nm due to localized HOMO–LUMO transitions of the triphenylamine moiety (Figure S2, Supporting Information).^[35] The close similarity of electronic levels of D3 and D4 are reflected both in the HOMO energy values (both ≈ 5.3 eV) as well as in the maximum absorption in the near-infrared region at ≈ 900 nm, which arises due

Table 1. HOMO energy E^{HOMO} values of neutral tris(4-bromophenyl)amine (TPA-Br₃), MeOTPD, and spiro-MeOTAD obtained by cyclic voltammetry (CV) half wave potential and differential pulse polarography (DPP) peak potential. Oxidation states of the corresponding peaks are given as (+x) in brackets. Ionization potential IP and workfunction WF were obtained by ultraviolet photoelectron spectroscopy on D2, D3, and D4.

Compound	CV ^(a)	DPP ^(a)	Compound	UPS ^(b)	
	$E^{\text{HOMO}}(+x)$			IP	WF
	[eV]	[eV]		[eV]	[eV]
TPA-Br ₃	-5.69(+I)	-5.81(+I)	D2	-5.67	-5.11
MeOTPD	-5.50(+I)	-5.51(+I)	D3	-5.34	-5.01
	-5.77(+II)	-5.76(+II)			
Spiro-MeOTAD	-5.38(+I)	-5.39(+I)	D4	-5.25	-4.91
	-5.53(+II)	-5.54(+II)			
	-5.75(+IV)	-5.75(+IV)			

^{a)} Measured in anhydrous dichloromethane (sample concentration 10^{-3} – 10^{-5} M) using, supporting electrolyte: 0.1 M TBAPF₆, reference electrode: Ag/AgNO₃, counter electrode: Platinum disk, and working electrode: platinum disk at a scan rate: 100 mV s⁻¹, at RT and ambient pressure. For DPP measurements, a pulse size of 20–50 mV with 100 ms pulse duration was chosen. The half wave potentials $E^{1/2}$ versus Ag/AgNO₃ were referenced to the vacuum level by $E^{\text{HOMO}}(\text{compound}) = [-e\{E^{1/2}(\text{compound vs ref. Ag/AgNO}_3) - (E^{1/2}(\text{Fc/Fc}^+ \text{ vs Ag/AgNO}_3))\}] + E^{\text{HOMO}}(\text{Fc/Fc}^+ \text{ vs } E_{\text{vac}}, \text{ solvent corrected})$. The ferrocene reference half-wave potential $E^{1/2}(\text{Fc/Fc}^+ \text{ vs Ag/AgNO}_3)$ was determined to be +0.10 V in DCM at a scan rate of 100 mV s⁻¹, $E_{\text{HOMO}}(\text{Fc/Fc}^+ \text{ vs } E_{\text{vac}}, \text{ solvent corrected})$ was taken as -5.16 eV.^[40] For complete dataset, see Table S1 of the Supporting Information; ^{b)} UPS was measured on 20 nm thin films of D2, D3, and D4 on ITO.

to optically induced hole transfer from the triarylamine unit to the linking bridge leading to this strong and broad absorption. This peak is obviously not visible in Magic Blue for the lack of any bridging units between the Ar₃N units.^[35] It is to be noted that D3 shows similar absorption signatures as a reported dication obtained from MeOTPD by oxidation using a silver salt of perfluorinated alkoxyaluminates.^[36] A small shoulder visible in the absorption spectrum of D2 at 630 nm is explained by symmetry breaking of the tris(4-bromophenyl)amine radical cation, which is not present in D3 and D4 due to their twisted arrangement of the phenyl groups around the nitrogen centers.^[36,37] In the Raman spectra of thin films (Figure S3, Supporting Information) typical aromatic hydrocarbon stretching vibrations are present; most notably, the C–H out-of-plane wagging from mono substituted benzene (908 cm⁻¹, Δ), C–H in plane bending from benzene rings (1175 cm⁻¹,*) and C–N stretching (1320 cm⁻¹, +) are observable. C–C stretching bands are susceptible to quinoid to benzoid transitions of the mesomeric structures. This explains the higher intensity of the more stabilized quinoid vibration in the biphenyl bridged cations, MeOTPD²⁺(PF₆)₂ and spiro-MeOTAD⁴⁺(PF₆)₄ (1564 cm⁻¹) as compared to the energetically more favored benzoid structure in the less stabilized Magic Blue (1606 cm⁻¹).^[36,38] The redox behavior and energy levels of our dopants and their pristine states are further studied by measuring the frontier orbitals using cyclic voltammetry (CV), as well as differential pulse polarography (DPP) by sequentially oxidizing the pristine molecules (Figure S4, Supporting Information). All the values are summarized in **Table 1**, together with the UPS values.

To avoid radical cross-coupling of the dopants, high scan rate was chosen for CV, which results in large peak-to-peak separation energies ΔE_p (Table S1, Supporting Information). All the pristine molecules show fully reversible redox cycles; the number of redox peaks depending on the number of nitrogen centres (Figure S4, Supporting Information). Obviously, TPA-Br₃ shows a single reversible oxidation, whereas MeOTPD exhibits two (mono- and dication) and spiro-MeOTAD three (mono-, di-, and tetracation) oxidation steps in both CV and DPP measurements. The mono-oxidation step of MeOTPD to MeOTPD¹⁺ and the dioxidation step of spiro-MeOTAD¹⁺ to spiro-MeOTAD²⁺ are almost degenerate in energy (-5.50 and -5.53 eV, respectively, in CV). This indicates that most probably, spiro-MeOTAD²⁺ resembles the monocation, MeOTPD¹⁺ electronically. Therefore, it can be deduced that spiro-MeOTAD²⁺ consists of two decoupled MeOTPD¹⁺ radical cations anchored at one common spiro carbon center, rather than a doubly charged MeOTPD²⁺ moiety linked to another neutral half. The chemical structures of all four possible spiro-MeOTAD oxidation states are compiled in Figure S5 of the Supporting Information. Moreover, both spiro-MeOTAD¹⁺ and MeOTPD¹⁺ possess sufficient low ionization potentials or E_{HOMO} of -5.38 and -5.50 eV, making exothermal multielectron electron transfer from P1 or P2 (IP = 4.6–4.7 eV) feasible to reach the zero oxidation states of both D3 and D4. The peak current obtained from the DPP experiment is directly related to the amount of electrons transferred and the concentration of the redox species, which is constant in our experiment.^[39] When comparing the differential pulse polarogram peak current of spiro-MeOTAD²⁺ and spiro-MeOTAD⁴⁺ signal, a two electron oxidation process from dication to tetracation can be inferred (Figure S4b, Supporting Information). This implies an intrinsically unstable triply charged spiro-MeOTAD³⁺, consistent with an earlier report by Zhang et al.^[40] Quantitative X-ray photoelectron spectroscopy analysis was employed to obtain the atomic composition (N/P) of D3 and D4 powder samples (see Table S2, Supporting Information). By comparing the theoretical nitrogen to phosphorous atomic ratios (N/P = 1 for both tetracation, D4 and dication D3) to experimentally determined nitrogen 1s and phosphorous 2p signal integral ratios (1.2 and 1.4, respectively), average contents of at least 60% for D3 and 80% for D4 can be assessed from XPS. Considering all the supporting data from CV, DPP, UPS, and XPS, it can be very well concluded that the di- and tetracation organic salts D3 and D4 were successfully synthesized, where both dopants are capable of exothermal multielectron transfer from the polymers P1 and P2.

2.2. Monitoring of the Doping Process

As a first step to study the charge transfer between dopants and polymers, we performed UV/vis/NIR absorption spectroscopy experiments, as it is a simple, yet powerful technique to probe changes in electronic states due to doping of polymers. Prior to chemical doping, the changes in spectral features of polymers P1 and P2 on electrochemical oxidation were determined by spectroelectrochemical (SEC) measurements in solution to identify the polaron features. For this, both polymers were biased from zero to +800 mV oxidation potential in 200 mV steps and absorption spectra are measured (Figure 2a). The ground-state

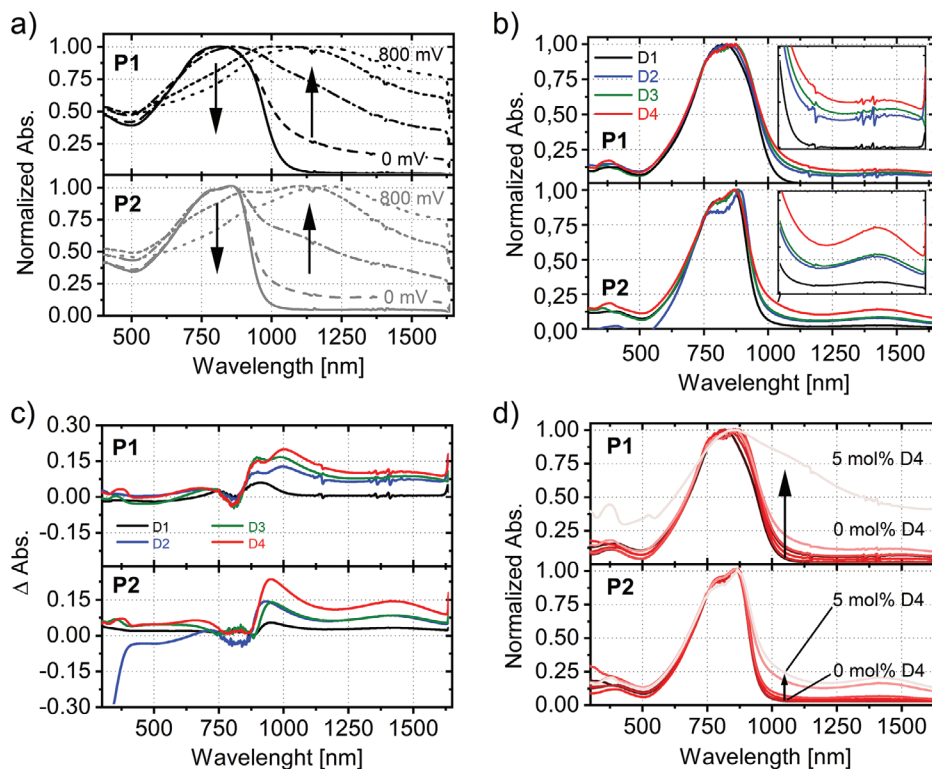


Figure 2. a) Spectroelectrochemical spectra of the polymers P1 and P2 in DCM obtained by biasing from 0 mV to +800 mV. A dedoping step of -100 mV was applied prior to measurement to ensure pristine polymer samples. b) Comparison of the optical absorption spectra of the doped P1 and P2 for four different dopants. D1–D4 at 2 mol% dopant loading in 0.01 mg mL $^{-1}$ polymer solution. c) Comparative difference spectra of both polymers with 2 mol% dopant loading, obtained by subtracting the pristine polymer absorption from the oxidized polymer absorption (b). d) Change in absorption for P1 on doping with 0 to 5 mol% D4 in DCM. Spectra (b–d) obtained under inert and anhydrous conditions.

absorptions for both P1 and P2 are located at 820 nm and upon electrochemical oxidation, the ground state absorption is bleached and new polaronic features appear at ≈ 1200 nm in the near-infrared region. The detailed absorption spectra for P1 and P2 for all the dopant concentrations ranging from 0.1 to 5 mol% for D1–D4 are shown in Figure S6 of the Supporting Information. Figure 2b shows the absorption spectra of chemically doped P1 and P2 for the four different dopants D1–D4 at a typical 2 mol% dopant concentration in 0.01 mg mL $^{-1}$ polymer solution. For both polymers, the MEAs, D3 and D4 show pronounced doping effects compared to the monovalent dopants D1 and D2. For all dopant concentrations, the TEG substituted polymer P1 exhibit the highest polaron absorption intensities in the increasing order from D2, over D3 to D4. Similarly, in the 2-hexyldecyl substituted polymer P2, a lower and less gradually expressed polaron absorption is observed with both D1 and D2. To delineate the changes in the absorption spectra, difference spectra were plotted in Figure 2c. Difference spectra are obtained by subtracting the spectrum of the pristine polymer from each spectrum of the doped polymers, thus emphasizing spectral changes upon doping. The upper plot in Figure 2c shows the difference spectra of the TEG substituted polymer P1 at a typical dopant concentration of 2 mol% for all four dopants. It shows a clear trend with increasing polaron intensity from D1 over D2 to D3 and D4. In the lower part, the difference plots for the alkyl substituted polymer P2 are shown. As before, only low doping

can be achieved using D1, and the intensity of the polaron absorption increases with the oxidation state of the dopants. A notable difference for P2 is that D1 and D2 yield similar and low polaron intensities, as compared to D3 and D4. For dopant molar ratios up to 2 mol% (Figure 2c), there is no other considerable difference between P1 and P2 in terms of polaron intensity. However, for the dopant D4, a higher absolute polaron absorption was measured in the case of the hydrophilic polymer P1 as compared to the hydrophobic derivative P2 at 5 mol% doping ratio (Figure 2d). This can be attributed probably due to better miscibility of D4 in the former at higher concentrations. Similar behavior was previously observed by Kroon et al., who doped ethylene glycol substituted polythiophenes using F $_4$ TCNQ and found an improved solubility and conductivity by the introduction of polar side chains.^[11] This can be explained as follows: for a successful molecular doping, the polar dopants must access the conjugated polymer backbone whereby the glycol substitution assists this mixing and therefore, a more steady and uniform doping process is attained with the more hydrophilic polymer P1.

Concomitant with polymer doping, the formation of reduced dopant species can be expected and consequently their original absorption changes. The pristine precursors (nonoxidized forms) of D2–D4 absorb only below 400 nm. To identify the optical signatures of intermediate reduction products of D3 and D4, i.e., MeOTPD $^+$ (PF $_6^-$) monocation and spiro-MeOTAD $^{2+}$ (PF $_6^-$) $_2$ dication salts, these were prepared by titration of their respective

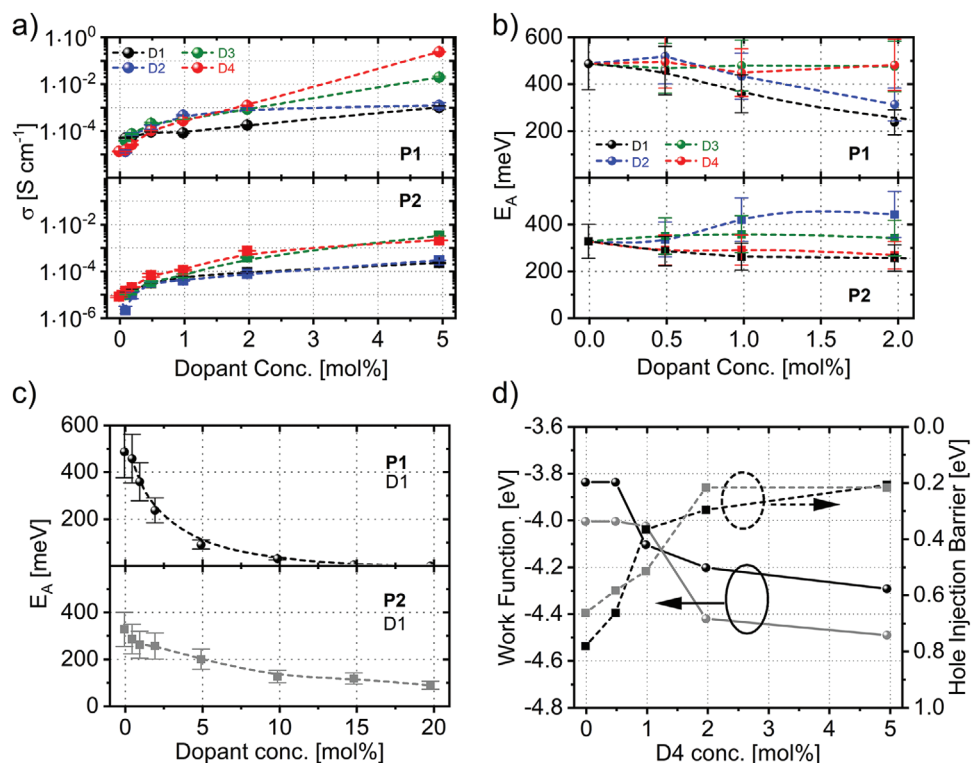


Figure 3. a) Electrical conductivity measurement. b) Evolution of the activation energies. c) E_A -progression of NOPF₆-doped films up to 20 mol% showing the drop of activation energy, which accompanies shift of the Fermi energy toward the transport level. d) Variation of work function (left y-axis, solid lines) and hole-injection barrier (right y-axis, dashed lines) of P1 (black) and P2 (gray) as a function of molar doping ratio from 0 to 5 mol% D4.

neutral precursors MeOTPD or spiro-MeOTAD using the necessary equivalents of oxidizing agents. Spectra of these salts can be found in Figure S2b of the Supporting Information. Both exhibit pronounced NIR absorption at ≈ 1500 nm with almost no absorption at 900 nm (typical absorption for the dopant D3 and D4, Figure S2a). Since the polaron absorption of P1 and P2 overlaps with the absorption of the reduced dopant intermediates at about 1500 nm, it is very difficult to elucidate the contribution of the reduced species toward near infrared absorption. It is to be noted that the contribution of the reduced species at low molar dopant regime is negligibly small. However, the increase in absorption below 400 nm can be attributed to the neutral triarylamine species of the dopants, even though the molar amount of the dopant used is very small. Nevertheless, it is valid to focus on the polaron absorptions for the first estimate of the doping process. It is clearly demonstrated, that D4 introduces a much higher polaron concentration than all other dopants for the whole dopant concentration up to 5 mol% in both polymers P1 and P2 studied here, regardless of the polarity of the polymer.

2.3. Impact on the Electrical Conductivity and Activation Energies

The above discussed absorption studies have proven the highly efficient doping of polymers by the multication salts in general and the highly pronounced nature of doping using D4. The coulombically bound polaron-counter ion pair can now release electrons upon thermal activation, thus increasing the bulk con-

ductivity. **Figure 3a** shows the electrical conductivity values of the doped systems measured in thin films in the range of zero to 5 mol% dopants for both the hydrophilic polymer P1 and the hydrophobic polymer P2. Interestingly, an increase in electrical conductivity over one to two orders of magnitude develops within 1 mol% of doping for any dopant for both P1 and P2. Below 1 mol% dopant concentrations, no big differences among the doping capabilities of D1–D4 are discernible. This initial strong increase of the conductivity at low doping concentrations is well-known in the literature and characteristic for filling of energetically deep lying states in highly disordered systems.^[41] On increasing dopant concentration, substantial differences for the four different dopants, as well as for the two polymers are evident. For example, above 1 mol%, the conductivity of doped P1 increases drastically for D3 and D4, whereas it levels off for D1 and D2, with the highest conductivity reached for the samples doped with D4 throughout the whole dopant concentration range. The final value for P1 doped with D3 reaches 1.9×10^{-2} S cm⁻¹ and with D4 0.2 S cm⁻¹ is obtained at 5 mol% dopant. In comparison, D1 and D2 increase the bulk conductivity of P1 to a mere 9.13×10^{-4} S cm⁻¹, and 1.12×10^{-3} S cm⁻¹, respectively (Tables S4 and S5, Supporting Information). Thus the tetracation salt D4 causes two orders and D3 results in one order of magnitude higher conductivity compared to monocation salts D1 and D2 at 5 mol% doping. In the hydrophobic polymer P2 also a strong increase in electrical conductivity is observed at lower dopant loadings, which however increases slower than in the hydrophilic polymer. This can be attributed to the lack of glycol-substitution leading

to a decreased accessibility of the polar dopants to the polymer backbones and therefore, to a lower efficiency of polaron formation in P2. In P2, D1 and D2 have an identically lower doping effect as compared to D3 and D4. Here, the final conductivity values at 5 mol% reach 1.8×10^{-4} and 2.3×10^{-4} S cm⁻¹ for D1 and D2, respectively, and 2.6×10^{-3} and 1.7×10^{-3} S cm⁻¹ for D3 and D4, respectively. Thus a distinctive difference between the low efficient monocation salts (D1, D2) and highly efficient multication salts (D3 and D4) can be observed with respect to the achieved conductivity values. Further, an increased polarity of the conjugated polymer in P1 facilitates the doping process.

To gain an understanding of the charge transport mechanism, the thermal activation energies of the conductivity in doped polymers were determined. The activation energies E_A were calculated from Arrhenius plots by measuring the temperature dependent conductivity $\sigma(T)$ for a range between room temperature and 100 °C. From the Arrhenius-plots (Figure S7, Supporting Information), the activation energy values E_A were extracted using the Arrhenius equation $\sigma(T) = \sigma_0 e^{-E_A/(k_B T)}$, where k_B is the Boltzmann constant. The activation energy obtained by this consists of two processes: a contribution for the charge transfer salt dissociation and the contribution of the thermally activated hopping, as described earlier by Schwarze et al.^[42] The activation for charge transfer dissociation, schematically shown in Equation (2), is typically at least one order of magnitude greater than the activation for hopping.^[42,43] Interestingly, we found drastic differences in E_A both, among the dopants, as well as between the two polymers. Figure 3b shows the activation energies of both doped polymers using different dopants for a dopant molar ratio up to 2 mol%. In the first glance, there is a distinct difference in behavior between NOPF₆ (D1) and the triarylamine cation salts (D2–D4). In the hydrophilic polymer P1, a steadily decreasing activation energy is obtained for D1 starting from 0 to 5 mol% (Figure 3b). This steady decline is very distinctive for an increased charge carrier density in organic semiconductors. By filling low lying, exponentially distributed trap states and shifting the Fermi level closer to the transport energy E_{Tr} , the hole injection barrier and the thermal activation energy for charge transport are lowered.^[17] E_{Tr} delimits the mobile from trapped charges, with only states higher in energy contributing to charge transport.^[44] The hydrophobic polymer P2 exhibits a comparable behavior, although the decrease of the activation energy upon doping with D1 proceeds much slower than for P1 (Figure 3b). This is also observable in the doping regime beyond 2 mol% (Table S4, Supporting Information) and it is explained with the inferior compatibility of the NOPF₆ salt with the hydrophobic polymer. In order to fully understand the steady decrease in E_A , for D1, we measured additionally the E_A for dopant concentrations up to 20 mol% of D1 for both P1 and P2. Figure 3c clearly shows, that E_A asymptotically approaches zero for 20 mol% D1.

The activation energy upon doping P2 with the oxidized triarylamine cations (D3–D4), which are HTM-dopants, remains, as in the polar polymer, almost constant. A slightly increasing activation energy is however found for D2 in polymer P2, which indicates an obstructed charge transport. On the contrary, in the case of the multication HTM-dopants D3 and D4, the activation energy for charge transport remains unchanged upon the intro-

duction of dopants. In the context of hopping transport, this indicates a relatively unchanged distance between Fermi- and transport level. UPS experiments on the polymers P1 and P2 doped with D4 (Figure 3d) confirm the downshift of E_F toward the respective HOMO, with a distinct pinning at 200 meV above the valence band maximum for both polymers. Since the transport levels E_{Tr} in a Gaussian density of states (DOS) remains fairly independent of the charge carrier concentration, the downshift of the Fermi level E_F seems to be compensated by the additional broadening of the DOS by doping.^[45] To determine the impact of the (partially or fully) reduced HTM-dopant compared to a non-HTM dopant on the HOMO density of states and their distribution in polymers, ultraviolet photoelectron spectroscopy was carried out on 20 nm thin films of undoped P1 and P2 and their doped samples with NOPF₆ (non-HTM dopant) and spiro-MeOTAD⁴⁺(PF₆⁻)₄ (HTM-dopant). After measurement of the valence band maximum (VBM), the onset was fitted with a modified exponential Gaussian distribution to account for localized/tail states arising due to ionized dopants (Equation (S10), Supporting Information). The broadening of the DOS was quantified by fitting Equation (S10) of the Supporting Information to the VBM (see also Figure 4a; numerical results summarized in Table S8, Supporting Information). A comparison of the standard deviation of the gaussian distribution of DOS (σ_{GDOS}) confirms that D1 ($\sigma_{GDOS} = 120$ meV) causes less change in the variance of the Gaussian part of the fit function than D4 ($\sigma_{GDOS} = 198$ meV) in P1. A similar broadening of DOS is observed in using an HTM-dopant like D4 in P2. Additionally, the most pronounced disorder, and exponential tailing of the pristine polymers was measured for the the polar TEG-substituted P1, which is consistent with the experimental observations made by Borsenberger and Bässler, that static dipole moments increase the energetic disorder in organic semiconducting systems.^[46] Together with the increased energetic disorder found via UPS experiments and the high number of dipoles (i.e., static disorder) added in the form of multiply charged small molecules, the constant activation energy for P1 and P2 using HTM-dopants can be attributed to a highly disordered system. However, at doping concentrations of 2 mol% and above, the use of multivalent dopants D3 and D4 result in doped polymers having conductivities orders of magnitude higher than D1 and D2. This advantage, however, comes along with the disadvantage, that a significant amount of static disorder is introduced by the highly charged HTM materials, causing no considerable decrease in activation energies for charge transport on increasing doping content.

Additionally, the difference in behavior of P1 and P2 toward the dopants can be explained as follows. As the ionization potential difference between P1 and P2 is almost negligible (≈ 0.05 eV), we do not expect the IP to cause any difference in the degree of ionization after doping by a significant amount. In addition, both polymers support an exothermic electron transfer to all dopants. Especially at higher doping ratios (i.e., 5 mol%), tail states should not impact the doping efficiency, as the Fermi level has well crossed all intragap and tail states at this point (Figure 3d). This leaves the polarity/side-chains as the only major difference in both polymers, as the possible cause for the difference in doping efficiency and ultimately the observed conductivity trend.

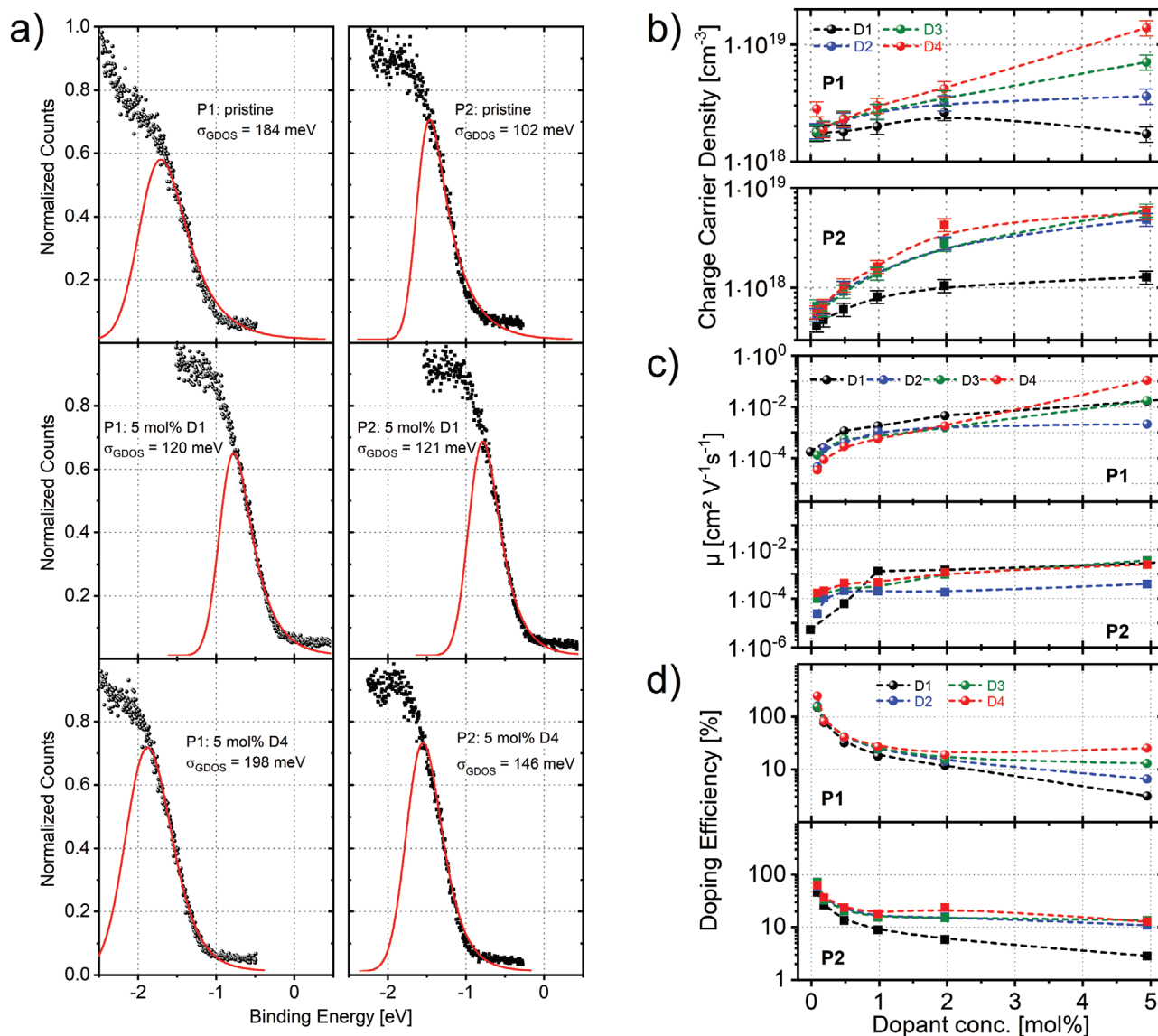


Figure 4. a) Valence band maxima of P1 and P2 doped with 0 mol% (top), 5 mol% D1 (center), and 5 mol% D4 (bottom) obtained from UPS and fitted with an exponentially modified Gaussian distribution (see Supporting Information for detailed calculation). p-doping with D4 induces a higher variance of the Gaussian distribution as compared to D1 doped polymers. b) Charge carrier density obtained from a calibration curve (see Supporting Information for details). c) Calculated charge carrier mobility μ of P1 and P2 doped with D1–D4, determined from Equation (1) using the measured charge carrier concentration and conductivity. Holes were assumed as the majority carrier type in the p-doped systems, neglecting electron contribution. d) Doping efficiency of the polymers P1 and P2, upon doping with the different dopants D1–D4. The doping efficiencies of D3 and D4 are normalized to 100% (denoting the uptake of two and four electrons, respectively).

2.4. Charge Carrier Density

The number of introduced charge carriers N_D is an important figure of merit in unipolar (p- or n-type) doped systems and is directly linked to the elementary charge e , the hole mobility μ_h and conductivity σ via Equation (1)

$$\sigma = e N_D \mu_h \quad (1)$$

In doped systems, N_D is conveniently accessible via capacitance–voltage (Mott–Schottky) experiments on metal–

insulator–semiconductor devices.^[26] In metal–insulator–semiconductor devices, holes are either accumulated or depleted at the semiconductor–insulator interface upon applying an electrical bias at the metal contact. Spatial width and capacitance of this depletion- or space-charge layer is, inter alia, very sensitive to the amount of ionized donors N_D present in the bulk. Using impedance spectroscopy, the change in depletion layer capacitance and consequently N_D of the doped system can be monitored (see Supporting Information for detailed information). Therefore, we have measured the charge carrier densities (N_D) of polymer films doped with D1 from 0 to 20 mol%

and correlated the resulting values with the respective polaron absorption intensities from optical absorption spectroscopy measurements. Since N_D correlates perfectly linear with the polaron peak integral obtained from UV/vis studies, a calibration curve can be obtained to deduce N_D , once the polaron intensity is measured (Figures S8 and S9, Supporting Information). Based on this calibration curve, the charge carrier densities for both polymer films doped with the other three dopants D2–D4 were read out from the polaron absorption values. Details regarding the method are elaborated in the respective section of the Supporting Information. For both polymers, for the whole range of dopant concentration, the doped samples using triarylamine dopants D2–D4 exhibit considerably higher N_D values compared to NOPF₆. The charge carrier densities in the doped hydrophilic polymer P1 scale with the oxidation state of the HTM-dopants; D4 doping exhibiting almost 3–5 times the value of D2 doping. Figure 4b shows this clear trend for P1 above 2 mol% dopant. At the highest concentration of 5 mol%, the anticipated scaling of the charge carrier density with the oxidation state is perfectly expressed: the monovalent dopant D2 creates a carrier density of $3.5 \times 10^{18} \text{ cm}^{-3}$, which doubles to $6.9 \times 10^{18} \text{ cm}^{-3}$ for D3 (dication) and quadruples for the fourfold oxidized D4, reaching a carrier density of $13.8 \times 10^{18} \text{ cm}^{-3}$. This correlation could not be observed in the doped hydrophobic polymer P2; indeed, the charge carrier density of D4 doped P2 films rises more strongly below 2 mol% dopant concentration, as compared to all the other dopants. Beyond 2 mol% in P2 however, the charge carrier densities generated by all three HTM-dopants D2–D4 merge and saturate reaching $5 \times 10^{18} \text{ cm}^{-3}$ at 5 mol%. This is still almost five times the value obtained for NOPF₆-doped P2. Thus, the HTM-dopants induce drastically higher carrier densities than D1, which affords a saturated value of only $1.2 \times 10^{18} \text{ cm}^{-3}$ at 5 mol%. The fact that for both, the polar polymer P1, and the nonpolar polymer P2, the redox dopant D1 performs worse than any of the HTM-dopants D2–D4 for the whole range of dopant concentrations up to 5 mol%, indicates the increased efficacy of doping conjugated polymers using triarylamine-cation based salts in general. Moreover, the higher the oxidation state of the dopant, the more efficient is the doping process.

2.5. Charge Carrier Mobility

The widely studied p-type dopants such as F₄TCNQ, and the fluorinated fullerene C₆₀F₃₆ are being reduced upon doping to form their anions such as F₄TCNQ⁻, and C₆₀F₃₆⁻, or charge transfer salts thereof.^[7] Typically, these reduced species do not contribute to the charge transport, or may even hamper it, ultimately resulting in reduced charge carrier mobilities. Our dopants D2–D4, consisting of oxidized triarylamine hole conductors, are able to transport charges in their pristine as well as partially oxidized states. The lower oxidized states (which are de facto the reduced dopant species after doping the polymer) are extensively used as charge transport layers for, e.g., solar cells.^[47] We therefore examined if the use of cation salts of hole conductors as dopants can have additional contributions toward charge transport within the host:dopant mixture, as compared to NOPF₆, which has no HTM component at all. For this, first

the zero-field charge carrier mobilities μ_0 of the pristine dopant precursors TPA-Br₃, MeOTPD, and spiro-MeOTAD were determined by impedance spectroscopy by fitting a Poole–Frenkel field-dependency (Figure S10a, Supporting Information). For this, negative differential susceptance measurements on hole-only FTO/semiconductor/Au devices were carried out. Holes are injected at one electrode if a sufficient electrical field F across the device is applied. By measuring the capacitive response of the biased device at different frequencies, an average carrier transit time for a given organic layer thickness and electrical field can be deduced. This ultimately yields μ_0 of the organic semiconductor after extrapolating $\mu(F)$ against zero electrical field. Details of calculation are published elsewhere and explained in the Supporting Information.^[26] It was found, that all the pristine compounds possess similar values of μ_0 (MeOTPD: $2.6 \times 10^{-3} \text{ cm}^2 \text{ V}^{-1} \text{ s}^{-1}$, followed by spiro-MeOTPD: $2.0 \times 10^{-3} \text{ cm}^2 \text{ V}^{-1} \text{ s}^{-1}$ and TPA-Br₃: $1.3 \times 10^{-3} \text{ cm}^2 \text{ V}^{-1} \text{ s}^{-1}$). Röhr et al. reported a similar value of $3.2 \times 10^{-3} \text{ cm}^2 \text{ V}^{-1} \text{ s}^{-1}$ for spiro-MeOTAD from space-charge limited current measurements.^[48] The impact of the HTM-dopants on charge carrier mobility of the doped polymer P1 and P2 was estimated by extracting the charge carrier mobility from the known parameters such as charge carrier density and conductivity using Equation (1). The results for both polymers doped with D1–D4 (0–5 mol%) are summarized in Figure 4c. Both, the polar P1 and the alkyl-substituted P2 improve in charge carrier mobility upon doping, regardless of the used dopant. This leads to the conclusion, that the presence of charged HTM dopants or their reduced products does not introduce trap states deeper in energy than already present in the disordered polymer semiconductor.^[49] This is substantiated by the measured activation energy, which remains virtually constant upon doping with D3 or D4 (Figure 3b). The more polar P1 shows signs of filling energetically low-lying tail states below the gaussian HOMO DOS (“trap-filling”), as evidenced by lowered activation energy in the case of D1 and D2. Trap-filling substantially increases the charge carrier mobility at low doping ratios, consistent with the mobility data shown in Figure 4c).^[17,22] The strong initial increase in μ_h tends to flatten more for the alkyl-substituted polymer P2 and is in agreement with the initial steep drop of the hole-injection barrier and the Fermi-level pinning at >2 mol% of D4 as seen in UPS experiments for both polymers (Figure 3d). When comparing the mobilities of the both doped polymers using the HTM dopants and NOPF₆, it appears that none of them affect the charge carrier mobility adversely and no considerable advantage is observed for the former, even though doping as such improves the charge carrier mobility.

2.6. Doping Efficiency

Besides fundamental electronic properties such as conductivity, charge carrier mobility, and charge carrier density, the doping efficiency (η_{Dop}) allows for comparison of our HTM-dopants versus NOPF₆. η_{Dop} is defined as the ratio of the number of free holes N_D (obtained by Mott–Schottky measurements) and the total number of dopant molecules N_A per unit volume. A higher η_{Dop} implies a more efficient dissociation of the bound charge transfer state formed by [Dopant^{(n-x)+}Polymer^{x+}] into

free majority charge carriers as given in Equation (2), where D and P stand for dopant and polymer, respectively.



One important point to note here is that the first step in the integer charge transfer doping reaction, i.e., the formation of the so-called charge transfer state is temperature independent.^[50] This implies, that nearly all dopants introduced into the system form ionized CT states, which are coulombically bound semiconductor–dopant pairs. In a second step, via thermal activation, free charge carriers responsible for the conductivity increase can be generated from the CT states. The ratio between the total amount of dopant molecules in the bulk versus free charge carriers can be understood as the doping efficiency. As evident from Figure 4d, the polar polymer P1 displays an exponential decrease in η_{Dop} at the lowest doping ratios, to below 25% ionization efficiency at 1 mol% dopant concentration. The pronounced loss in carrier generation efficiency with an increasing amounts of dopant molecules is known in the literature for organic semiconductors. It can be explained by a free hole capture process by ionized dopant molecules, which become statistically more likely, the more dopant is present in the system.^[22] Accumulation of unreacted dopant was detected in the absorption spectra for the highest doping concentration of 5 mol% D4 at 380 nm in Figure 2d. Consistent with our electrical conductivity and UV/vis/NIR absorption studies, the more hydrophobic polymer P2 overall hinders the charge transfer salt dissociation, resulting in lower doping efficiency. This can be traced back to a decreased accessibility of the polymer backbone for dopant molecules and molecular miscibility. Ethylene glycol polar side chains are known to improve the dopant miscibility and doping efficacy for donor–acceptor copolymers.^[51–53] Further, a large relative permittivity ϵ_r introduced by the TEG sidechains ($\epsilon_r(\text{P1}) = 5.41$) helps to overcome Coulomb interaction of the charge transfer salt compared to the alkyl-substituted P2 with $\epsilon_r(\text{P2}) = 4.74$ (Figure S10b, Supporting Information, for detailed calculation of dielectric constants). In both polymers, D4 offers the highest ratio of dissociated to total dopant molecules, closely followed by D3. To conclude, multivalent oxidized HTM dopants offer an advantage in carrier generation efficiency from their charge transfer salts compared to Magic Blue and NOPF₆, which especially manifests itself at high dopant concentrations of >2 mol%.

3. Conclusion

We synthesized novel and stable HTM-dopants, dication (MeOTPD²⁺(PF₆⁻)₂, D3) and tetracation (spiro-MeOTAD⁴⁺(PF₆⁻)₄, D4) salts and comparatively studied their use as p-dopants or MEAs for two conjugated polymers belonging to the class of PDPPs differing in their polarity and dielectric constants. Their superiority over conventional one-electron oxidants such as NOPF₆ (D1) and Magic Blue (D2) for p-doping was clearly proven. We observed a fourfold amount of positively charged polarons in both polymers when using the tetracationic salt D4, resulting in a higher electrical conductivity and charge carrier density as compared to equivalent molar amounts of mono and divalent dopants. Unlike NOPF₆ (D1),

a higher amount of energetic disorder is introduced in the density of states of doped polymer by MeOTPD²⁺(PF₆⁻)₂ and spiro-MeOTAD⁴⁺(PF₆⁻)₄, resulting in higher activation energies for charge transport. No negative effects on the charge carrier mobility were observed due to the presence of these dopants or their reduced species. Finally, the doping efficiency of D4 remains the highest among all the dopants for the whole range of dopant concentration from 0 to 5 mol%. Thus, a highly efficient method of generating charge carriers in conjugated polymers is demonstrated using multiply charged salts of triarylamine derivatives to help decrease the dopant loading necessary for achieving strongly improved electronic properties, thereby overcoming issues associated with excess use of dopants. Synergistic effects between multivalent HTM dopants and hydrophilic polymers further boost the doping efficiencies. Our findings pave the way for a new and highly efficient route of doping conjugated polymers using MEA cation salts.

Supporting Information

Supporting Information is available from the Wiley Online Library or from the author.

Acknowledgements

G.K. and A.H. contributed equally to this work. The authors kindly acknowledge financial support from the Deutsche Forschungsgemeinschaft (SPP TH807/8-1) and Bavarian Ministry of State for Science and Arts (Solar Technologies Go Hybrid, SolTech). The authors acknowledge Dr. Holger Schmalz for providing the Raman data and the instrument facility, the confocal WITec alpha 300 RA+ imaging system equipped with a UHTS 300 spectrometer. The XPS/UPS facility (PHI 5000 VersaProbe III system) at the Keylab Device Engineering in Bavarian Polymer Institute, University of Bayreuth is also acknowledged. After initial online publication, Table 1 was corrected on November 18, 2021, due to incorrect formatting. The editorial office apologizes for any convenience caused.

Open access funding enabled and organized by Projekt DEAL.

Conflict of Interest

The authors declare no conflict of interest.

Data Availability Statement

Data available on request from the authors.

Keywords

doping, electron transfer, polymers, radical ions, semiconductors

Received: July 23, 2021
Revised: September 23, 2021
Published online: October 22, 2021

- [1] B. H. Lee, G. C. Bazan, A. J. Heeger, *Adv. Mater.* **2016**, 28, 57.
- [2] Y. Hu, Z. D. Rengert, C. McDowell, M. J. Ford, M. Wang, A. Karki, A. T. Lill, G. C. Bazan, T.-Q. Nguyen, *ACS Nano* **2018**, 12, 3938.
- [3] Y. Kim, S. Chung, K. Cho, D. Harkin, W.-T. Hwang, D. Yoo, J.-K. Kim, W. Lee, Y. Song, H. Ahn, Y. Hong, H. Sirringhaus, K. Kang, T. Lee, *Adv. Mater.* **2019**, 31, 1806697.

- [4] I. H. Jung, C. T. Hong, U.-H. Lee, Y. H. Kang, K.-S. Jang, S. Y. Cho, *Sci. Rep.* **2017**, *7*, 44704.
- [5] H. Yan, J. G. Manion, M. Yuan, F. P. García De Arquer, G. R. Mckeown, S. Beaupré, M. Leclerc, E. H. Sargent, D. S. Seferos, *Adv. Mater.* **2016**, *28*, 6491.
- [6] Y. Zhang, H. Zhou, J. Seifert, L. Ying, A. Mikhailovsky, A. J. Heeger, G. C. Bazan, T.-Q. Nguyen, *Adv. Mater.* **2013**, *25*, 7038.
- [7] H. Hase, I. Salzmänn, in *Handbook of Organic Materials for Electronic and Photonic Devices*, 2nd ed. (Ed: O. Ostroverkhova), Woodhead Publishing, Oxford, UK **2019**, pp. 349–383.
- [8] I. Salzmänn, G. Heimel, M. Oehzelt, S. Winkler, N. Koch, *Acc. Chem. Res.* **2016**, *49*, 370.
- [9] J. Hynynen, D. Kiefer, L. Yu, R. Kroon, R. Munir, A. Amassian, M. Kemerink, C. Müller, *Macromolecules* **2017**, *50*, 8140.
- [10] B. Lüssem, M. Riede, K. Leo, *Phys. Status Solidi A* **2013**, *210*, 9.
- [11] R. Kroon, D. Kiefer, D. Stegerer, L. Yu, M. Sommer, C. Müller, *Adv. Mater.* **2017**, *29*, 1700930.
- [12] Y. Karpov, T. Erdmann, M. Stamm, U. Lappan, O. Guskova, M. Malanin, I. Raguzin, T. Beryozkina, V. Bakulev, F. Günther, S. Gemming, G. Seifert, M. Hamsbsch, S. Mannsfeld, B. Voit, A. Kiri, *Macromolecules* **2017**, *50*, 914.
- [13] H. Li, E. Plunkett, Z. Cai, B. Qiu, T. Wei, H. Chen, S. M. Thon, D. H. Reich, L. Chen, H. E. Katz, *Adv. Electron. Mater.* **2019**, *5*, 1800618.
- [14] Y. Xuan, X. Liu, S. Desbief, P. Leclère, M. Fahlman, R. Lazzaroni, M. Berggren, J. Cornil, D. Emin, X. Crispin, *Phys. Rev. B* **2010**, *82*, 115454.
- [15] D. Kiefer, R. Kroon, A. I. Hofmann, H. Sun, X. Liu, A. Giovannitti, D. Stegerer, A. Cano, J. Hynynen, L. Yu, Y. Zhang, D. Nai, T. F. Harrelson, M. Sommer, A. J. Moulé, M. Kemerink, S. R. Marder, I. McCulloch, M. Fahlman, S. Fabiano, C. Müller, *Nat. Mater.* **2019**, *18*, 149.
- [16] G. Chauhan, R. Srivastava, A. Kumar, O. Rana, P. C. Srivastava, M. N. Kamalasanan, *Org. Electron.* **2012**, *13*, 394.
- [17] S. Olthof, S. Mehraeen, S. K. Mohapatra, S. Barlow, V. Coropceanu, J.-L. Brédas, S. R. Marder, A. Kahn, *Phys. Rev. Lett.* **2012**, *109*, 176601.
- [18] I. E. Jacobs, E. W. Aasen, J. L. Oliveira, T. N. Fonseca, J. D. Roehling, J. Li, G. Zhang, M. P. Augustine, M. Mascal, A. J. Moulé, *J. Mater. Chem. C* **2016**, *4*, 3454.
- [19] F. Deschler, D. Riedel, A. Deák, B. Ecker, E. Von Hauff, E. Da Como, *Synth. Met.* **2015**, *199*, 381.
- [20] J. Euvrard, A. Revaux, P.-A. Bayle, M. Bardet, D. Vuillaume, A. Kahn, *Org. Electron.* **2018**, *53*, 135.
- [21] V. I. Arkhipov, E. V. Emelianova, P. Heremans, H. Bässler, *Phys. Rev. B* **2005**, *72*, 235202.
- [22] M. L. Tietze, L. Burtone, M. Riede, B. Lüssem, K. Leo, *Phys. Rev. B* **2012**, *86*, 035320.
- [23] B. Tan, S. R. Raga, A. S. R. Chesman, S. O. Furer, F. Zheng, D. P. Mcmeekin, L. Jiang, W. Mao, X. Lin, X. Wen, J. Lu, Y.-B. Cheng, U. Bach, *Adv. Energy Mater.* **2019**, *9*, 1901519.
- [24] W. H. Nguyen, C. D. Bailie, E. L. Unger, M. D. McGehee, *J. Am. Chem. Soc.* **2014**, *136*, 10996.
- [25] W. Zhang, F. Zhang, B. Xu, Y. Li, L. Wang, B. Zhang, Y. Guo, J. M. Gardner, L. Sun, L. Kloo, *ACS Appl. Mater. Interfaces* **2020**, *12*, 33751.
- [26] M. Goel, M. Siegert, G. Krauss, J. Mohanraj, A. Hochgesang, D. C. Heinrich, M. Fried, J. Pflaum, M. Thelakkat, *Adv. Mater.* **2020**, *32*, 2003596.
- [27] A. I. Hofmann, R. Kroon, S. Zokaei, E. Järsvall, C. Malacrida, S. Ludwigs, T. Biskup, C. Müller, *Adv. Electron. Mater.* **2020**, *6*, 2000249.
- [28] P. Schmode, A. Savva, R. Kahl, D. Ohayon, F. Meichsner, O. Dolynchuk, T. Thurn-Albrecht, S. Inal, M. Thelakkat, *ACS Appl. Mater. Interfaces* **2020**, *12*, 13029.
- [29] G. Krauss, F. Meichsner, A. Hochgesang, J. Mohanraj, S. Salehi, P. Schmode, M. Thelakkat, *Adv. Funct. Mater.* **2021**, *31*, 2010048.
- [30] C. J. Mueller, E. Gann, C. R. Singh, M. Thelakkat, C. R. McNeill, *Chem. Mater.* **2016**, *28*, 7088.
- [31] B. Meng, J. Liu, L. Wang, *Polym. Chem.* **2020**, *11*, 1261.
- [32] B. Meng, H. Song, X. Chen, Z. Xie, J. Liu, L. Wang, *Macromolecules* **2015**, *48*, 4357.
- [33] H. Méndez, G. Heimel, A. Opitz, K. Sauer, P. Barkowski, M. Oehzelt, J. Soeda, T. Okamoto, J. Takeya, J.-B. Arlin, J.-Y. Balandier, Y. Geerts, N. Koch, I. Salzmänn, *Angew. Chem., Int. Ed.* **2013**, *52*, 7751.
- [34] I. Salzmänn, G. Heimel, S. Duhm, M. Oehzelt, P. Pingel, B. M. George, A. Schnegg, K. Lips, R.-P. Blum, A. Vollmer, N. Koch, *Phys. Rev. Lett.* **2012**, *108*, 035502.
- [35] C. Lambert, G. Nöll, *J. Am. Chem. Soc.* **1999**, *121*, 8434.
- [36] Y. Su, X. Wang, X. Zheng, Z. Zhang, Y. Song, Y. Sui, Y. Li, X. Wang, *Angew. Chem., Int. Ed.* **2014**, *53*, 2857.
- [37] S. Amthor, B. Noller, C. Lambert, *Chem. Phys.* **2005**, *316*, 141.
- [38] C. Kvarnström, A. Petr, P. Damlin, T. Lindfors, A. Ivaska, L. Dunsch, *J. Solid State Electrochem.* **2002**, *6*, 505.
- [39] D. J. Myers, J. Osteryoung, *Anal. Chem.* **1973**, *45*, 381.
- [40] W. Zhang, L. Wang, Y. Guo, B. Zhang, V. Leandri, B. Xu, Z. Li, J. M. Gardner, L. Sun, L. Kloo, *Chem. Commun.* **2020**, *56*, 1589.
- [41] A. Fediai, F. Symalla, P. Friederich, W. Wenzel, *Nat. Commun.* **2019**, *10*, 4547.
- [42] M. Schwarze, C. Gaul, R. Scholz, F. Bussolotti, A. Hofacker, K. S. Schellhammer, B. Nell, B. D. Naab, Z. Bao, D. Spoltore, K. Vandewal, J. Widmer, S. Kera, N. Ueno, F. Ortman, K. Leo, *Nat. Mater.* **2019**, *18*, 242.
- [43] H. Matsui, D. Kumaki, E. Takahashi, K. Takimiya, S. Tokito, T. Hasegawa, *Phys. Rev. B* **2012**, *85*, 035308.
- [44] J. O. Oelerich, F. Jansson, A. V. Nenashev, F. Gebhard, S. D. Baranovskii, *J. Phys.: Condens. Matter* **2014**, *26*, 255801.
- [45] B. Hartenstein, H. Bässler, *J. Non-Cryst. Solids* **1995**, *190*, 112.
- [46] P. M. Borsenberger, H. Bässler, *J. Chem. Phys.* **1991**, *95*, 5327.
- [47] Z. Hawash, L. K. Ono, Y. Qi, *Adv. Mater. Interfaces* **2018**, *5*, 1700623.
- [48] J. A. Röhr, X. Shi, S. A. Haque, T. Kirchartz, J. Nelson, *Phys. Rev. Appl.* **2018**, *9*, 044017.
- [49] S.-J. Yoo, J.-H. Lee, J.-H. Lee, J.-J. Kim, *Appl. Phys. Lett.* **2013**, *102*, 183301.
- [50] M. L. Tietze, J. Benduhn, P. Pahner, B. Nell, M. Schwarze, H. Kleemann, M. Krammer, K. Zojer, K. Vandewal, K. Leo, *Nat. Commun.* **2018**, *9*, 1182.
- [51] D. Kiefer, A. Giovannitti, H. Sun, T. Biskup, A. Hofmann, M. Koopmans, C. Cendra, S. Weber, L. J. Anton Koster, E. Olsson, J. Rivnay, S. Fabiano, I. McCulloch, C. Müller, *ACS Energy Lett.* **2018**, *3*, 278.
- [52] J. Liu, L. Qiu, R. Alessandri, X. Qiu, G. Portale, J. Dong, W. Talsma, G. Ye, A. A. Sengrian, P. C. T. Souza, M. A. Loi, R. C. Chiechi, S. J. Marrink, J. C. Hummelen, L. J. A. Koster, *Adv. Mater.* **2018**, *30*, 1704630.
- [53] J. Liu, G. Ye, H. G. O. Potgieser, M. Koopmans, S. Sami, M. I. Nugraha, D. R. Villalva, H. Sun, J. Dong, X. Yang, X. Qiu, C. Yao, G. Portale, S. Fabiano, T. D. Anthopoulos, D. Baran, R. W. A. Havenith, R. C. Chiechi, L. J. A. Koster, *Adv. Mater.* **2021**, *33*, 2006694.